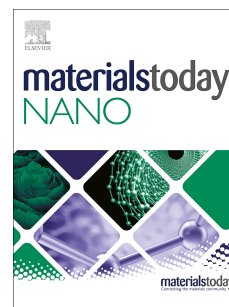


Journal Pre-proof

Piezo-Phototronic Effect Boosted Catalysis in Plasmonic Bimetallic ZnO Heterostructure with Guided Fermi Level Alignment

Yalong Zhang, Shaobo Wang, Yunchao Zhao, Yiming Ding, Zeyu Zhang, Tao Jiang, Zhong Lin Wang, Linlin Li



PII: S2588-8420(22)00005-0

DOI: <https://doi.org/10.1016/j.mtnano.2022.100177>

Reference: MTNANO 100177

To appear in: *Materials Today Nano*

Received Date: 24 November 2021

Revised Date: 3 January 2022

Accepted Date: 24 January 2022

Please cite this article as: Zhang Y., Wang S., Zhao Y., Ding Y., Zhang Z., Jiang T., Wang Z.L. & Li L., Piezo-Phototronic Effect Boosted Catalysis in Plasmonic Bimetallic ZnO Heterostructure with Guided Fermi Level Alignment, *Materials Today Nano*, <https://doi.org/10.1016/j.mtnano.2022.100177>.

This is a PDF file of an article that has undergone enhancements after acceptance, such as the addition of a cover page and metadata, and formatting for readability, but it is not yet the definitive version of record. This version will undergo additional copyediting, typesetting and review before it is published in its final form, but we are providing this version to give early visibility of the article. Please note that, during the production process, errors may be discovered which could affect the content, and all legal disclaimers that apply to the journal pertain.

© 2022 Elsevier Ltd. All rights reserved.

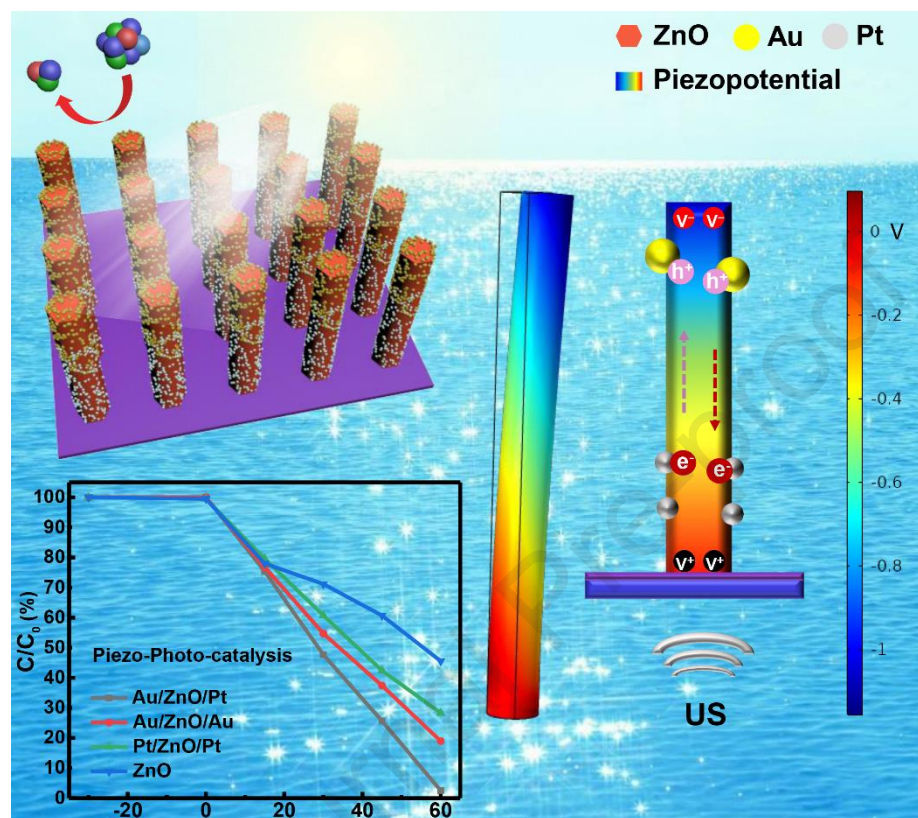
CRedit authorship contribution statement

Yalong Zhang and Shaobo Wang contributed equally. **Yalong Zhang:** Investigation, Methodology, Data curation, Formal analysis, Writing -original draft. **Shaobo Wang:** Investigation, Methodology, Data curation, Formal analysis. **Yunchao Zhao:** Methodology. **Yiming Ding:** Methodology. **Zeyu Zhang:** Methodology. **Tao Jiang:** Supervision, Writing - review& editing. **Zhong Lin Wang:** Supervision, Resources, Writing - review& editing. **Linlin Li:** Supervision, Conceptualization, Resources, Project administration, Funding acquisition, Writing - review & editing.

Journal Pre-proof

Graphical Abstract

Piezo-Phototronic Effect Boosted Catalysis in Plasmonic Bimetallic ZnO Heterostructure with Guided Fermi Level Alignment



A plasmonic bimetallic ZnO nanorod array (Au/ZnO/Pt) was fabricated with Au nanoparticles (NPs) located on top of ZnO nanorods and Pt NPs evenly distributed on the ZnO nanorods. With the rational design integrating guided Fermi level alignment and piezo-phototronic effect, the piezo-photocatalytic efficiency is greatly boosted.

Piezo-Phototronic Effect Boosted Catalysis in Plasmonic Bimetallic ZnO Heterostructure with Guided Fermi Level Alignment

Yalong Zhang^{1,2†}, Shaobo Wang^{1,2†}, Yunchao Zhao^{1,2}, Yiming Ding^{1,2}, Zeyu Zhang^{1,2}, Tao Jiang^{1,2,3*}, Zhong Lin Wang^{1,2,3,4*}, Linlin Li^{1,2,3*}

¹Center on Nanoenergy Research, School of Resources, Environment and Materials, Guangxi University, Nanning 530004, P. R. China

²Beijing Institute of Nanoenergy and Nanosystems, Chinese Academy of Sciences, Beijing 101400, P. R. China

³University of Chinese Academy of Sciences, Beijing 100049, P. R. China

⁴School of Materials Science and Engineering, Georgia Institute of Technology, Atlanta, GA 30332-0245, USA

† Y.Z. and S.W. contributed equally to this work.

* Corresponding author: jiangtao@binn.cas.cn (Tao Jiang); zhong.wang@mse.gatech.edu (Zhong Lin Wang); lilinlin@binn.cas.cn (Linlin Li)

Abstract

High photoinduced carriers (PC) recombination rate, low PC mobility and limited solar energy utilization rate are the three main roadblocks that severely limit the photocatalytic activity of semiconductors. In this work, we designed a plasmonic bimetallic ZnO nanorod array (Au/ZnO/Pt) with Au nanoparticles (NPs) located on top of ZnO nanorods, and Pt NPs evenly distributed on the ZnO nanorods for improving catalysis through the piezo-phototronic effect. With the rational design of guided Fermi level alignment, the photoinduced hot electrons of Au NPs with localized surface plasmon resonance (LSPR) effect can transfer to Pt NPs through ZnO to promote the separation and migration of PC. More importantly, under the stimulation of ultrasound, ZnO with piezo-phototronic effect generates an interfacial piezo-potential, thereby further promoting the separation and transport of carriers in compliance with the direction of piezo-potential to promote the surface redox reaction. Under the synergy of piezo-phototronic effect and LSPR effect, the Au/ZnO/Pt (AZP) realized 97.5% dye degradation in 60 min, which was 1.2, 1.36 and 1.79 folds of that with Au/ZnO/Au (AZA), Pt/ZnO/Pt (PZP) and ZnO, respectively. The unique plasmonic bimetallic heterostructure with piezo-phototronic effect and guided Fermi level alignment can guide the directional migration of carriers and provides useful instruction for the design of high-efficiency catalysts.

Keywords: piezo-potential, piezo-phototronic effect, localized surface plasmon resonance, piezo-photocatalysis, nanorod array

1. Introduction

With the rapid economic growth, energy and environmental issues have become increasingly prominent. Industrial and sanitary water pollution represents the most serious pollution problem worldwide. [1, 2] As a green, energy-saving and simple method, photocatalysis with semiconductor (SC) photocatalysts has been widely used in water pollution treatment for freshwater availability. [3-9] The artificial photocatalytic process over a SC can be mainly divided into three stages: photoactivation, charge separation and translocation, and final surface anodic and cathodic redox reactions for degradation of pollutants. [10] In this process, low solar energy utilization rate, low carrier mobility, and high photoinduced electron-hole recombination rate are the three main roadblocks that severely limit the photocatalytic efficiency. [11] Aim at solving these problems, different methods have been developed to improve the catalysis from the aspect of material engineering, including building heterojunction to promote interfacial carrier transportation and separation, [12] atom-level modifying or doping to modulate reactive centers, [13] constructing ultrathin structure to shorten carrier mobility pathway, etc. [14-16] However, these methods might narrow the band gap of the whole catalyst, thus reducing the redox potential of the catalyst to react with pollutants. Therefore, strategies that can simultaneously broaden light utilization and promote carrier separation without reducing the redox potential are more attractive. [10, 17, 18] For instance, formation of Schottky junction between plasmonic metal and semiconductor with rational Fermi level alignment can not only broaden light utilization, but also promote the generation and separation of carriers for finally improving photocatalysis. [19-22] However, it is still far from optimal to realize a rapid and efficient water decontamination.

Recently, piezoelectric SCs have brought new blood to traditional photocatalysis with their unique piezotronic and piezo-phototronic effect. [23] Piezoelectric nanomaterials, such as wurtzite ZnO and perovskite BaTiO₃ have relative displacement of the crystal centers of cations and anions under an external mechanical stress, bringing forth dipole polarization and piezo-potential, which can continuously renew the built-in electric field. [24] It can further act as a powerful driving force for modulating the transport and separation of PC that are generated in the photocatalytic process, thus boosting the catalytic efficiency. [25] For instance, it has been found that the construction of Schottky heterostructures from a plasmonic metal and a

piezoelectric SC, such Au/ZnO, Ag/BaTiO₃, and Ag/Ag₂S/BaTiO₃ [26, 27] have improved catalytic efficiency under the co-stimulation of the sunlight and a mechanical force. It is due to that under the action of mechanical force to generate the interfacial piezo-potential, the increase of barrier height promoted the separation of carriers and promoted their transport along the direction of piezo-potential. [28] In contrast, the position with decreased barrier height may hinder the separation of carriers. [29] It is inevitable that the piezocatalyst uniformly supported by the plasma metal strengthens the PC separation at one side of the piezo-potential and weakens the PC separation at the other side. Thus, rational construction of the heterostructures with proper Fermi level alignment, along with its positive corporation with directional piezo-potential, can finally determine the boost of catalysis. [22] For instance, the combination of two metals with different work functions and a SC might guide the directional migration of carriers along with the alignment of the Fermi level. [22]

Based on these considerations, herein, we designed a plasmonic bimetallic ZnO heterostructure with one-dimensional (1D) nanowire array structure (abbr. as AZP) to boost the piezo-photocatalysis. The ZnO nanorods grown on the substrate has uniaxial (C-axis) piezoelectricity no matter of the direction of external mechanical force (Figure S1, supporting information). The plasmonic Au NPs were located on the top end of the ZnO nanorods and Pt NPs were evenly distributed on the ZnO nanorods. The formation of a pair of Schottky junction of Au/ZnO and Pt/ZnO with Fermi level alignment promoted the separation of carriers under photoexcitation. Moreover, the external ultrasound triggered piezo-potential of ZnO at the Au/ZnO and Pt/ZnO interfaces acted as the robust promoter to trap electrons and extend the life of carriers. As a result, the catalytic degradation of a model pollutant methyl orange (MO) improved by 45% and 70% relative to mere photocatalysis and mere piezocatalysis, respectively. In comparison, the bimetallic ZnO heterostructure had a higher catalytic efficiency than the monometallic ones, AZA and PZP. This design proposes an alternative strategy for improving the separation of PC for photocatalysts via the photo-piezotronic effect.

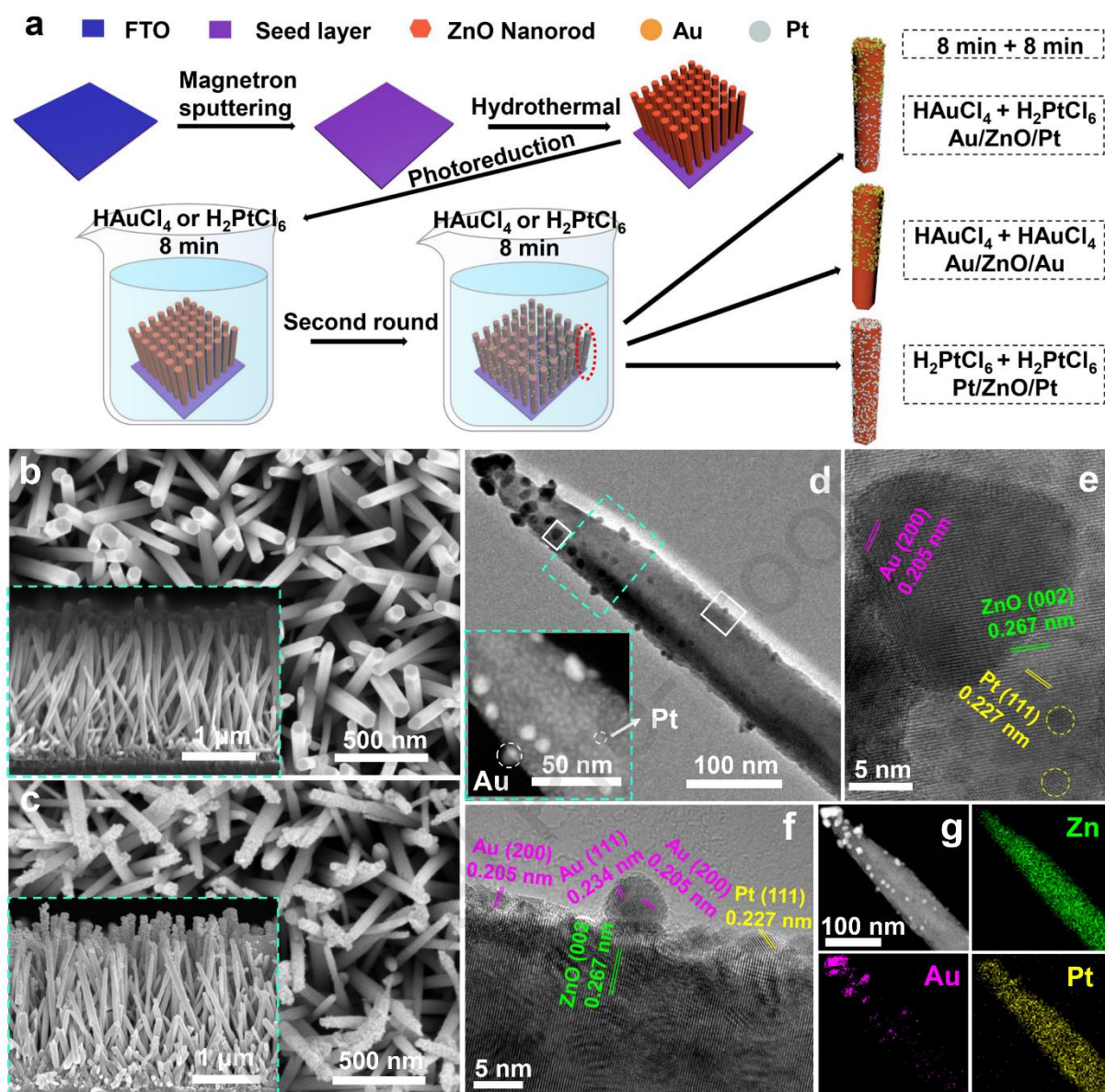


Figure 1. The synthesis process of the nanocatalysts and their structures. (a) Preparation process of the nanocatalysts. SEM images showing overhead view of (b) the ZnO and (c) the AZP nanorod array. The insets in (b) and (c) show the corresponding side view. (d) TEM image of the AZP nanorod array with well-defined boundary (inset). (e) and (f) HRTEM images of the AZP nanorod. (g) EDX element mapping of the AZP nanorod.

2. Results and Discussions

The preparation process of the nanocatalysts including AZA, PZP, and AZP nanorod arrays are shown in Figure 1a. On a fluorine-doped tin oxide (FTO) substrate, ZnO nanorod array was firstly grown through a hydrothermal method. Then, Au NPs or Pt NPs were deposited on the vertically grown ZnO nanorods through photo-reduction using HAuCl_4 or H_2PtCl_6 as the metal precursors, respectively. The second round of photo-reduction with corresponding noble metal

precursors generated AZP, AZA or PZP nanorod array. From the scanning electron microscope (SEM) images showing the overhead view and cross-sectional morphology of the ZnO nanorods (Figure 1b), the nanorods were vertically and closely grown on the FTO glass with diameter of about 75 nm and length of about 2000 nm, the large-scale SEM image shows the good uniformity of the ZnO nanorod array (Figure S3, Supporting Information). Figure 1c shows the typical SEM image of the AZP nanorod array, in which a lot of small NPs were grown on the surface of the nanorods. From the transmission electron microscope (TEM) and high-resolution TEM (HRTEM) images of a single AZP nanorod scraped from the FTO substrate, many small NPs existed and the NPs had different sizes (Figure 1d and S4, Supporting Information). The lattice fringes of 2.67 Å was assigned to the (002) facets of wurtzite ZnO; those of 2.05 Å and 2.36 Å were assigned to the (111) and (200) facets of cubic Au, respectively; and those of 2.27 Å and 1.96 Å were assigned to the (111) and (200) facets of cubic Pt, respectively (Figure 1e and 1f). The Au NPs were mainly distributed on the top end of the ZnO nanorod with diameter of 15 ± 5 nm, and Pt NPs were uniformly distributed on the whole ZnO nanorod with smaller size of 4 ± 1 nm. The energy dispersive x-ray spectroscopy (EDX) for element mapping also showed similar trend of element distribution (Figure 1g, S5c and S6c, Supporting Information). The SEM and TEM images of the monometallic heterostructure AZA and PZP are given in supporting information (Figure S2, S5 and S6, Supporting Information). The different size of Au and Pt NPs through similar photoreduction process can be attributed to the different crystallization properties of these two kinds of metal. [30]

In the X-ray diffraction (XRD) patterns of these catalysts, the diffraction peaks of the samples corresponded to the wurtzite structured ZnO (JCPDS No. 36-1451) (Figure S7, Supporting Information). No peaks belonging to other phases including Pt and Au were observed in the several heterostructured samples, due to the low content of Pt and Au. X-ray photoelectron spectroscopy (XPS) was used to detect the elements and their valences (Figure S8, S9 and S10, Supporting Information). From the high-resolution Zn 2p spectra (Figure S8b, S9a and S10a, Supporting Information), all the samples of AZP, AZA, and PZP had the two peaks centered at 1021.5 and 1044.6 eV, attributed to the existence of Zn 2p_{3/2} and Zn 2p_{1/2}, respectively. In the high-resolution Au4f spectra of AZP and AZA (Figure S8c and S9b, Supporting Information), the two double lines at 83.67 and 87.32eV were assigned to metal Au 4f_{7/2} and Au 4f_{5/2}, respectively, corresponding to the binding energies of Au⁰. The double peaks near the Au 4f region at 88.3 and 91.2 eV were assigned to Zn 3p_{3/2} and Zn 3p_{1/2}, respectively. In the high-resolution Pt 4f spectra for AZP and PZP (Figure S8d and S10b, Supporting Information), peaks at 70.7/72.13/74.81 eV and 74.05/75.48/78.16 eV were assigned to the metal Pt 4f_{7/2} and Pt 4f_{5/2},

respectively, associated with binding energies of Pt^0 , Pt^{2+} and Pt^{4+} , respectively. The existence of Pt^{2+} and Pt^{4+} valences was due to the existence of Pt-O bond on the Pt NPs. [31] The oxidation state of Pt usually appears on small Pt NPs due to that the oxygen chemisorption can easily happen at surface step and kink sites of NPs. [32, 33] Interestingly, in the AZP, the peak for low-valence Pt including Pt^0 and Pt^{2+} was obvious than that of PZP, which was caused by the accumulation of more electrons on the Pt side. By comparing the peak positions of binding energy of AZA and PZP (Table S1, Supporting Information), the Au $4f_{7/2}$ and Pt $4f_{7/2}$ peaks in the AZP were nearly unchanged, revealing that the Au and Pt NPs were co-decorated on the ZnO, and no Au-Pt alloy was formed. The piezoelectricity of AZP and ZnO were also confirmed by the voltage response amplitude-voltage curve under a 10 V direct current bias field (Figure S11, Supporting Information). The piezoelectric coefficient d_{33} was calculated to be about 80 pm V^{-1} from the slope of the piezoresponse amplitude-voltage curve.

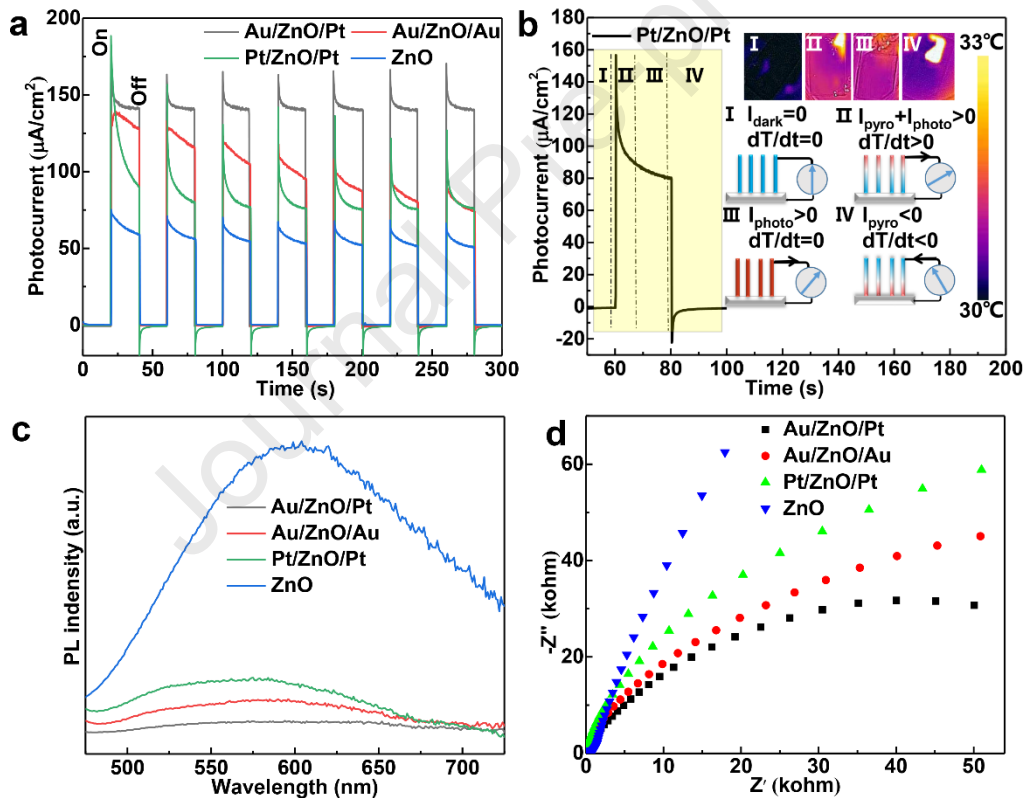


Figure 2. Photoelectrochemical properties of the samples. (a) Time-dependent photocurrent density of the AZP, AZA, PZP and ZnO nanorod array under full-spectrum light irradiation. (b) Pyroelectric process of PZP with the corresponding inset showing infrared thermal imaging. (c) Photoluminescence spectra and (d) EIS Nyquist plots of ZnO, AZP, AZA and PZP nanorod array.

The photocurrent of the catalysts under full-spectrum light irradiation is shown in Figure 2a. The photocurrent for all the three kinds of heterostructured nanorod array was improved compared with ZnO. Especially, AZP showed the highest photocurrent density reaching $141.3 \mu\text{A cm}^{-2}$, which was about 1.4, 1.56 and 2 folds of that of AZA, PZP and ZnO, respectively. Moreover, AZP showed the highest photocurrent stability under the repeated on-off of the light irradiation, due to that Pt NPs acted as a promoter to trap electrons and prolong the life of carriers. In comparison, AZA, PZP and ZnO suffered from decreased photocurrent with the repeated on-off of the light irradiation. It was worth noting that there was a rising peak of each photocurrent peak when the illuminant was turned on and a peak falling when the illuminant was turned off. It demonstrated that the pyroelectric effect of ZnO contributed to the photocurrent [34]. The pyroelectric current (j) can be calculated according the equations (1-3),

$$j = -\partial P_s / \partial t = -(\partial P_s / \partial T)(\partial T / \partial t) \quad (1)$$

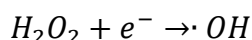
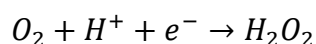
$$\text{let } p = -(\partial P_s / \partial T) \quad (2)$$

$$j = p(\partial T / \partial t) \quad (3)$$

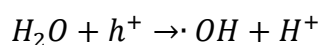
where P_s is the saturation polarization, p is the pyroelectric coefficient that is a constant, T represents the temperature, and t is the light irradiation time. So, $j \propto dT/dt$. From the thermal infrared images in the upper inset of Figure 2b, the local temperature changed instantaneously (increased from 30 to 31 °C when the light on and then decreased to 30 °C when the light off). When the light was turned off (Figure 2b I), there was no temperature change on the ZnO surface ($dT/dt=0$), so the pyroelectric current was 0 ($I_{\text{dark}}=0$). When the light was turned on (Figure 2b II), the loaded plasmonic metal NPs (Au and Pt) can convert the optical energy of light into local heat and cause the temperature increase ($dT/dt>0$), so the pyroelectric current appeared ($I_{\text{pyro}}>0$, $I_{\text{photo}}>0$) [35]. With the prolonging of the irradiation time (Figure 2b III), the local temperature reached a stable level ($dT/dt=0$), so the pyroelectric current returned to 0 ($I_{\text{pyro}}=0$, $I_{\text{photo}}>0$). Then, when the light turned off instantaneously (Figure 2b IV), ZnO released heat and caused the surface temperature drop ($dT/dt<0$), so the pyroelectric current decreased to 0 ($I_{\text{pyro}}<0$, $I_{\text{photo}}=0$).

As shown in Figure S12 a inset, AZP and AZA showed LSPR shoulder peaks at about 520 nm contributed from Au NPs, whereas there was no observable peak in the visible light region for ZnO and PZP. According to the Tauc plot, the direct band gaps of AZP, AZA, PZP and ZnO were calculated to be 3.20, 3.23, 3.20 and 3.24 eV, respectively. Therefore, the light absorption of the catalysts was mainly confined within the UV region (Figure S12b, Supporting Information). The Mott–Schottky plot of AZP, AZA, PZP and ZnO recorded at 1 kHz are presented in figure S12 c. The flat band energy of AZP, AZA, PZP and ZnO are 0.02, 0.02,

0.01 and -0.09 V (vs. Ag/AgCl), respectively. Thus, the calculated C_B of Au/ZnO/Pt, AZP, AZA, PZP and ZnO are 0.32, 0.32, 0.31 and 0.21 eV, respectively (the detailed calculation is shown in the Supporting information). The calculated V_B of AZP, AZA, PZP and ZnO are 3.52, 3.55, 3.51 and 3.45 eV, respectively. The conduction band level of all the catalysts is more negative than the reduction potential of O_2/H_2O_2 (+0.69 eV), so the following reactions can occur on the conduction band:



The valence band level of all the catalysts is more positive than the reduction potential of $H_2O/\cdot OH$ (+2.38 eV), so the following reactions can occur on the valence band:



In order to further prove the production of the above reaction, terephthalic acid was used to detect $\cdot OH$, and the fluorescence of the corresponding 2-hydroxyterephthalic acid at 426 nm confirmed the production of $\cdot OH$ (Figure S13a, Supporting Information). The potassium iodide (KI) detection method was used to detect the presence of H_2O_2 , and the change in the absorption spectrum of I^{3-} at 360 nm confirmed the production of H_2O_2 (Figure S13b, Supporting Information). Therefore, the explanation of the degradation mechanism is shown in Figure S13c.

The photoluminescence spectroscopy was characterized to study the photocarrier separation ability of the catalysts (Figure 2c). Under the 325 nm light excitation, AZP had much lower intensity of the emission peak at about 570 nm relative to the others, revealing that the more efficient separation of PC in the AZP heterojunction. This result was consistent with that of the photocurrent stability (Figure 2a). These results confirmed the highest photoelectric conversion ability of AZP. Electrochemical impedance spectroscopy (EIS) was used to uncover the carrier transport behavior near the heterojunction region (Figure 2d). In the Nyquist diagram, the larger the radius of curvature of the arc, the greater the transfer resistance of the interface charge [36]. The AZP heterojunction had the smallest radius of curvature, indicating that it had the lowest PC transfer resistance.

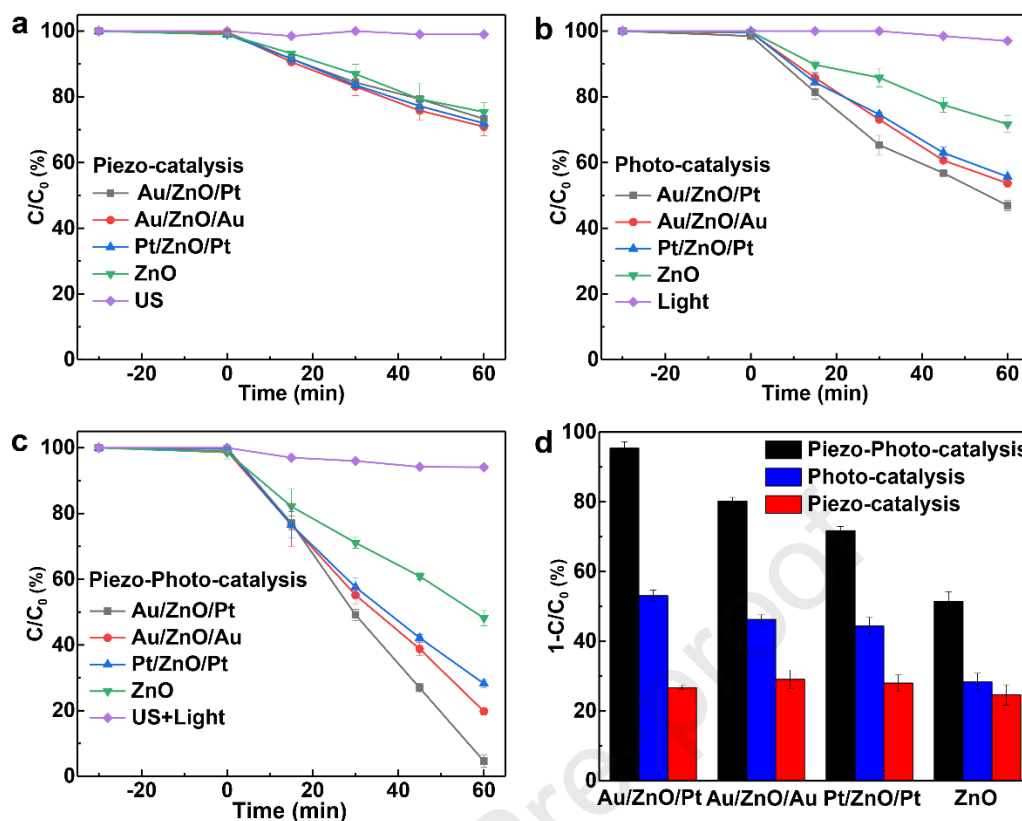


Figure 3. Degradation of MO with AZP, AZA, PZP and ZnO. (a) Piezocatalysis under ultrasound. (b) Photocatalysis under full-spectrum light irradiation. (c) Piezo-photocatalysis under both ultrasound and light irradiation. (d) Statistics of the piezo-photocatalysis, photocatalysis, and piezocatalytic degradation for 60 min with AZP, AZA, PZP, and ZnO.

In order to assess the catalytic performance of these nanocatalysts, we used MO as a model dye molecule of wastewater pollutant and detected its degradation under ultrasound (40 kHz, 80 W), full-spectrum light irradiation (2 W cm^{-2}), and both ultrasound and light irradiation, respectively (Figure 3). Figure 3a shows the catalytic activity of different nanocatalysts under ultrasound stimulation. The catalytic activity was defined as $C/C_0 \cdot 100 \%$ and the corresponding degradation rate was defined as $(1-C/C_0) \cdot 100 \%$, where C_0 is the MO concentration at $T=0$ min when the adsorption equilibrium is reached and C is the MO concentration after catalysis ($T=60$ min). With only the ultrasound triggered piezoelectric effect for catalysis, the degradation rate for all the nanocatalysts was lower than 30%, indicating that the polarization charges generated by ZnO under the mechanical stress of ultrasonic cavitation had a low catalytic efficiency. Under the full-spectrum light irradiation, degradation of MO was 25% for ZnO, and it increased for about 17-28% for the heterostructured samples, with AZP showing the highest degradation rate of 52% (Figure 3b). The reason was deduced as follows: The catalytic efficiency of pure ZnO under light stimulation was limited due to the rapid

recombination of PC. With the formation of Schottky junction with Au NPs (or Pt NPs), Au NPs (or Pt NPs) caused collective oscillations of the surface electrons under the light excitation, namely local plasma oscillation, which was then converted into hot electrons being injected into ZnO to inhibit the recombination of carriers. As a result, the monometallic PZP and AZA heterostructures had similar degradation efficiency on MO. When the Au NPs and Pt NPs were simultaneously uploaded onto ZnO to form a bimetallic heterostructure, the degradation rate of MO was increased to 52%. Under all-spectrum light irradiation, Au NPs located on the top of ZnO generated collective oscillation of surface electronics to trigger the LSPR effect, which then generated hot electrons. The Pt NPs acted as a cocatalysts to trap electrons, prolonging the life of carriers and further improving the catalytic efficiency. Interestingly, under the co-stimulation of the ultrasound and the all-spectrum light, the degradation rate of MO was greatly increased. The degradation rate of MO with AZP, AZA, PZP and ZnO reached 97.5%, 81%, 72% and 54%, respectively. Due to the participation of ultrasonic vibration, ZnO can generate a piezoelectric polarization or called built-in electric field along its C-axis. This built-in electric field enhanced the separation and transport of PC at the interface of Schottky junction by adjusting the bending of the energy band, further increasing the degradation rate (Figure 3c). The degradation rate of each catalyst under various conditions is shown in Figure 3d. AZP showed obvious degradation advantages under the synergistic effect of ultrasound and light. Here, the enhancement index of photocatalytic efficiency by piezo-phototronic effect is defined as: $\text{piezo-photocatalytic efficiency}/(\text{piezocatalytic efficiency}+\text{photocatalytic efficiency})$. The calculated enhancement index of AZP, AZA, PZP and pure ZnO by piezo-phototronic effect was 1.23, 1.06, 1.02 and 1.13, respectively. After three cycles of catalysis under the co-stimulation of ultrasound and light, the MO degradation efficiency of AZP was 97.5%, 94.4% and 94.2%, respectively (Figure S16, Supporting Information). Moreover, the morphology of AZP did not show obvious change after piezo-photocatalysis, indicating its high catalytic stability (Figure S17, Supporting Information).

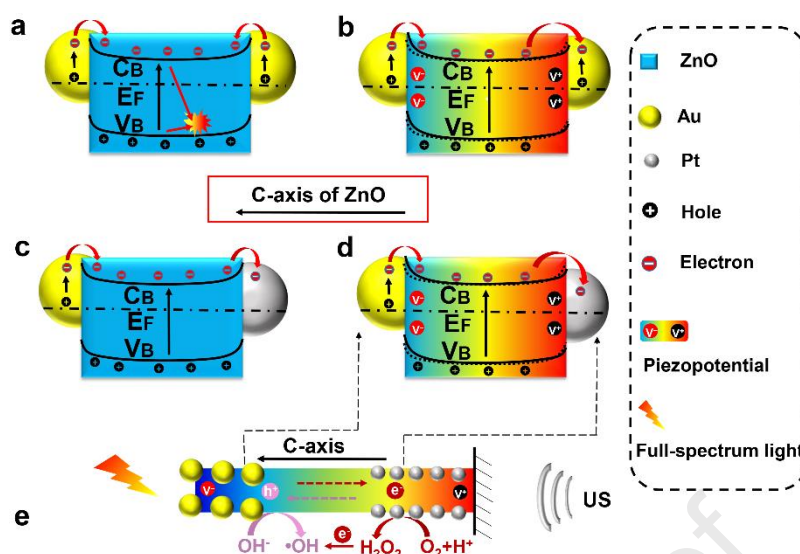


Figure 4. Mechanism for the enhanced catalysis by piezo-phototronic effect and the unique structure under both ultrasound and light irradiation. C_B and V_B represent C_B and V_B of ZnO, respectively; E_F represents energy of the Fermi level). (a) AZA under light irradiation. (b) AZA under both ultrasound and light irradiation. (c) AZP under light irradiation. (d) and (e) AZP under both ultrasound and light irradiation.

To better understand the enhanced catalytic activity of the bimetallic ZnO heterostructure compared with the monometallic ZnO heterostructure and pure ZnO, especially under the co-stimulation of light and ultrasound, the corresponding energy band structure is analyzed (**Figure 4**). For photocatalysis under the all-spectrum light, the visible light is mainly absorbed by the metal NPs (Au or Pt), while ZnO with wide band gap can only absorb the UV light. Due to its limited light absorption and low carrier separation rate, the photocatalytic efficiency of pure ZnO is low. [37] For AZA, Schottky junction is form between Au NPs and ZnO with the different Fermi levels of Au and ZnO. The Schottky barrier can trap electrons in the C_B of ZnO to inhibit the recombination of the carriers. Under the light irradiation, the excited hot electrons from plasmonic Au NPs can cross the Schottky barrier and reach the C_B of ZnO, leaving the same number of holes on Au to participate in the oxidation degradation of MO. At the same time, the electrons in the V_B of ZnO transport to its C_B to form PC (Figure 4a and S18a). Thus, the photocatalysis of Au/ZnO was improved compared with pure ZnO. However, with the continuous enrichment of electrons in the V_B of ZnO, the separation of carriers on ZnO will be gradually inhibited. It is the main reason that the photocurrent of AZA decreased with prolonged time as shown in Figure 2a. Under the external stress from the ultrasonic cavitation, ZnO will generate piezo-potential along the C-axis, which helps to further promote the separation of PC. In addition, the photoinduced electrons and holes are transported along the

opposite directions of piezo-potential, promoting the reduction and oxidation reaction, respectively (Figure 4b). [38] When Au and Pt NPs are simultaneously loaded onto ZnO to form a bimetallic heterostructure, the charge carriers will redistribute at the interfaces because of the different work function of Au, Pt and ZnO with the sequence of Pt (5.5 eV) > Au (5.1 eV) > ZnO (4.7 eV). [39] It assists in the diffusion of electrons from ZnO to Au and Pt, forming a pair of Schottky barrier at the contact interfaces of Au/ZnO and Pt/ZnO. Electron can transfer from Au to Pt through ZnO due to the Fermi level of Pt is lower than that of Au. For the AZP, under the light irradiation, the hot electrons of Au traverse the Schottky barrier and reach the C_B of ZnO. At the same time, the photoinduced electrons of ZnO transfer from the V_B to the C_B and move toward Pt NPs, which act as an electron acceptor to promote the PC separation (Figure 4c and S18b). The piezo-potential of ZnO under the external stress generates negative polarization charge at the Au/ZnO interface, causing an upward band bending of ZnO at the interface to promote the separation of PC. It also generates positive polarization charges at the Pt/ZnO interface, causing a downward band bending of ZnO at this interface to promote the photoinduced electrons to migrate to Pt, thereby promoting the separation of the carriers. With the piezo-phototronic effect, the carrier transport is in accordance with the direction of piezo-potential, [40] in which the photoinduced electrons are transported along the negative direction of the piezo-potential, and the photoinduced holes are transported along the positive direction of the piezo-potential (Figure 4d and S1). [41] It finally greatly promotes the carrier separation and boost the surface catalytic reaction through the advanced oxidation processes for highly efficient organic pollutant degradation (Figure 4e).

3. Conclusion

In conclusion, the plasmonic bimetallic AZP nanorod array was successfully designed with the guided Fermi level alignment. Importantly, under the ultrasound, ZnO with piezo-phototronic effect can generate piezo-potential at the interface of the Au/ZnO and Pt/ZnO Schottky junctions, inducing the band bending of ZnO at the interfaces with opposite directions to promote the separation of PC along the guided Fermi level alignment. The direction of the promoted carrier transport was in compliance with the direction of piezo-potential. When the ultrasound and light were applied together, the catalytic degradation of model pollutant with AZP increased by 1.2, 1.36 and 1.79 folds relative to AZA, PZP and ZnO, respectively. The unique one-dimensional bimetallic heterostructure with the piezo-phototronic effect and guided Fermi level alignment has guiding significance for the design of high-efficiency catalysts.

4. Experimental Section

Preparation of AZP, AZA and PZP Nanorod Array: Au and Pt NPs were deposited in sequence on ZnO through a photoreduction reaction under irradiation by a UV lamp. For example, for the fabrication of Au/ZnO/Pt, ZnO immersed in $\text{HAuCl}_4 \cdot 4\text{H}_2\text{O}$ (0.09 mM) was light-irradiated for 8 min to obtain Au/ZnO. Then, the Au/ZnO immersed in $\text{H}_2\text{PtCl}_6 \cdot 6\text{H}_2\text{O}$ (0.09 mM) was light-irradiated for 8 min to obtain AZP. The other monometallic samples AZA and PZP were prepared following the similar procedures. The details about the reagents, synthesis of samples, characterizations and photoelectrochemical measurements are introduced in the Supplementary file.

Acknowledgements

The work was supported by the National Key R&D project from Minister of Science and Technology, China (2016YFA0202703), the National Nature Science Foundation (No. 82072065, and 81471784), and the National Youth Talent Support Program.

Appendix A. Supplementary Data

Supporting information is available in the online version of this article.

Data availability

The raw/processed data required to reproduce these findings cannot be shared at this time as the data also forms part of an ongoing study.

References

- [1] R.P. Schwarzenbach, B.I. Escher, K. Fenner, T.B. Hofstetter, C.A. Johnson, U.v. Gunten, B. Wehrli, The Challenge of Micropollutants in Aquatic Systems, *Science*, 313 (2006) 1072-1077.
- [2] M.S. Mauter, I. Zucker, F. Perreault, J.R. Werber, J.-H. Kim, M. Elimelech, The role of nanotechnology in tackling global water challenges, *Nature Sustainability*, 1 (2018) 166-175.
- [3] A. Fujishima, K. Honda, Electrochemical Photolysis of Water at a Semiconductor Electrode, *Nature*, 238 (1972) 37-38.
- [4] C.V. Reddy, I.N. Reddy, R. Koutavarapu, K.R. Reddy, T.A. Saleh, T.M. Aminabhavi, J. Shim, Novel edge-capped ZrO_2 nanoparticles onto V_2O_5 nanowires for efficient photosensitized reduction of chromium (Cr (VI)), photoelectrochemical solar water splitting, and electrochemical energy storage applications, *Chemical Engineering Journal*, 430 (2022) 132988.

- [5] R. Koutavarapu, M.R. Tamtam, S.-G. Lee, M.C. Rao, D.-Y. Lee, J. Shim, Synthesis of 2D NiFe₂O₄ nanoplates/2D Bi₂WO₆ nanoflakes heterostructure: An enhanced Z-scheme charge transfer and separation for visible-light-driven photocatalytic degradation of toxic pollutants, *Journal of Environmental Chemical Engineering*, 9 (2021) 105893.
- [6] R. Koutavarapu, K. Syed, S. Pagidi, M.Y. Jeon, M.C. Rao, D.-Y. Lee, J. Shim, An effective CuO/Bi₂WO₆ heterostructured photocatalyst: Analyzing a charge-transfer mechanism for the enhanced visible-light-driven photocatalytic degradation of tetracycline and organic pollutants, *Chemosphere*, 287 (2022) 132015.
- [7] R. Koutavarapu, C.V. Reddy, K. Syed, K.R. Reddy, T.A. Saleh, D.-Y. Lee, J. Shim, T.M. Aminabhavi, Novel Z-scheme binary zinc tungsten oxide/nickel ferrite nanohybrids for photocatalytic reduction of chromium (Cr (VI)), photoelectrochemical water splitting and degradation of toxic organic pollutants, *Journal of Hazardous Materials*, 423 (2022) 127044.
- [8] M. Mousavi, A. Habibi-Yangjeh, M. Abitorabi, Fabrication of novel magnetically separable nanocomposites using graphitic carbon nitride, silver phosphate and silver chloride and their applications in photocatalytic removal of different pollutants using visible-light irradiation, *Journal of Colloid and Interface Science*, 480 (2016) 218-231.
- [9] S.J. Lee, H.J. Jung, R. Koutavarapu, S.H. Lee, M. Arumugam, J.H. Kim, M.Y. Choi, ZnO supported Au/Pd bimetallic nanocomposites for plasmon improved photocatalytic activity for methylene blue degradation under visible light irradiation, *Applied Surface Science*, 496 (2019) 143665.
- [10] X. Xue, W. Zang, P. Deng, Q. Wang, L. Xing, Y. Zhang, Z.L. Wang, Piezo-potential enhanced photocatalytic degradation of organic dye using ZnO nanowires, *Nano Energy*, 13 (2015) 414-422.
- [11] S. Tu, Y. Guo, Y. Zhang, C. Hu, T. Zhang, T. Ma, H. Huang, Piezocatalysis and Piezo-Photocatalysis: Catalysts Classification and Modification Strategy, Reaction Mechanism, and Practical Application, *Adv. Funct. Mater.*, 30 (2020) 2005158.
- [12] Q. Xu, L. Zhang, B. Cheng, J. Fan, J. Yu, S-Scheme Heterojunction Photocatalyst, *Chem*, 6 (2020) 1543-1559.
- [13] H. Huang, S. Tu, C. Zeng, T. Zhang, A.H. Reshak, Y. Zhang, Macroscopic Polarization Enhancement Promoting Photo- and Piezoelectric-Induced Charge Separation and Molecular Oxygen Activation, *Angew. Chem. Int. Ed.*, 56 (2017) 11860-11864.
- [14] F. Chen, T. Ma, T. Zhang, Y. Zhang, H. Huang, Atomic-Level Charge Separation Strategies in Semiconductor-Based Photocatalysts, *Adv. Mater.*, 33 (2021) 2005256.

- [15] J. Hu, L. Yu, J. Deng, Y. Wang, K. Cheng, C. Ma, Q. Zhang, W. Wen, S. Yu, Y. Pan, J. Yang, H. Ma, F. Qi, Y. Wang, Y. Zheng, M. Chen, R. Huang, S. Zhang, Z. Zhao, J. Mao, X. Meng, Q. Ji, G. Hou, X. Han, X. Bao, Y. Wang, D. Deng, Sulfur vacancy-rich MoS₂ as a catalyst for the hydrogenation of CO₂ to methanol, *Nature Catalysis*, 4 (2021) 242-250.
- [16] Y. Chen, L. Su, M. Jiang, X. Fang, Switch type PANI/ZnO core-shell microwire heterojunction for UV photodetection, *Journal of Materials Science & Technology*, 105 (2022) 259-265.
- [17] H. Guan, G. Mao, T. Zhong, T. Zhao, S. Liang, L. Xing, X. Xue, A self-powered UV photodetector based on the hydrovoltaic and photoelectric coupling properties of ZnO nanowire arrays, *Journal of Alloys and Compounds*, 867 (2021) 159073.
- [18] Z. Wang, T. Hu, H. He, Y. Fu, X. Zhang, J. Sun, L. Xing, B. Liu, Y. Zhang, X. Xue, Enhanced H₂ Production of TiO₂/ZnO Nanowires Co-Using Solar and Mechanical Energy through Piezo-Photocatalytic Effect, *ACS Sustainable Chemistry & Engineering*, 6 (2018) 10162-10172.
- [19] Z. Liu, W. Hou, P. Pavaskar, M. Aykol, S.B. Cronin, Plasmon Resonant Enhancement of Photocatalytic Water Splitting Under Visible Illumination, *Nano Lett.*, 11 (2011) 1111-1116.
- [20] S. Mubeen, G. Hernandez-Sosa, D. Moses, J. Lee, M. Moskovits, Plasmonic Photosensitization of a Wide Band Gap Semiconductor: Converting Plasmons to Charge Carriers, *Nano Lett.*, 11 (2011) 5548-5552.
- [21] A. Tanaka, S. Sakaguchi, K. Hashimoto, H. Kominami, Preparation of Au/TiO₂ with Metal Cocatalysts Exhibiting Strong Surface Plasmon Resonance Effective for Photoinduced Hydrogen Formation under Irradiation of Visible Light, *ACS Catalysis*, 3 (2013) 79-85.
- [22] A. Tanaka, K. Nakanishi, R. Hamada, K. Hashimoto, H. Kominami, Simultaneous and Stoichiometric Water Oxidation and Cr(VI) Reduction in Aqueous Suspensions of Functionalized Plasmonic Photocatalyst Au/TiO₂-Pt under Irradiation of Green Light, *ACS Catalysis*, 3 (2013) 1886-1891.
- [23] W. Wu, C. Pan, Y. Zhang, X. Wen, Z.L. Wang, Piezotronics and piezo-phototronics – From single nanodevices to array of devices and then to integrated functional system, *Nano Today*, 8 (2013) 619-642.
- [24] Z.L. Wang, Piezotronic and Piezophototronic Effects, *The Journal of Physical Chemistry Letters*, 1 (2010) 1388-1393.
- [25] Z. Liu, X. Yu, L. Li, Piezopotential augmented photo- and photoelectro-catalysis with a built-in electric field, *Chinese Journal of Catalysis*, 41 (2020) 534-549.

- [26] S. Xu, L. Guo, Q. Sun, Z.L. Wang, Piezotronic Effect Enhanced Plasmonic Photocatalysis by AuNPs/BaTiO₃ Heterostructures, *Adv. Funct. Mater.*, 29 (2019) 1808737.
- [27] Y. Lei, S. Xu, M. Ding, L. Li, Q. Sun, Z.L. Wang, Enhanced Photocatalysis by Synergistic Piezotronic Effect and Exciton–Plasmon Interaction Based on (Ag-Ag₂S)/BaTiO₃ Heterostructures, *Adv. Funct. Mater.*, 30 (2020) 2005716.
- [28] L. Pan, S. Sun, Y. Chen, P. Wang, J. Wang, X. Zhang, J.-J. Zou, Z.L. Wang, Advances in Piezo-Phototronic Effect Enhanced Photocatalysis and Photoelectrocatalysis, *Advanced Energy Materials*, 10 (2020) 2000214.
- [29] W. Wu, Z.L. Wang, Piezotronics and piezo-phototronics for adaptive electronics and optoelectronics, *Nature Reviews Materials*, 1 (2016) 16031.
- [30] L.K. Ono, B. Yuan, H. Heinrich, B.R. Cuenya, Formation and Thermal Stability of Platinum Oxides on Size-Selected Platinum Nanoparticles: Support Effects, *The Journal of Physical Chemistry C*, 114 (2010) 22119-22133.
- [31] Z. Zhang, A. Li, S.-W. Cao, M. Bosman, S. Li, C. Xue, Direct evidence of plasmon enhancement on photocatalytic hydrogen generation over Au/Pt-decorated TiO₂ nanofibers, *Nanoscale*, 6 (2014) 5217-5222.
- [32] A.S. Aricò, A.K. Shukla, H. Kim, S. Park, M. Min, V. Antonucci, An XPS study on oxidation states of Pt and its alloys with Co and Cr and its relevance to electroreduction of oxygen, *Appl. Surf. Sci.*, 172 (2001) 33-40.
- [33] Y. Ding, Y. Wang, L. Zhang, H. Zhang, C.M. Li, Y. Lei, Preparation of TiO₂–Pt hybrid nanofibers and their application for sensitive hydrazine detection, *Nanoscale*, 3 (2011) 1149-1157.
- [34] D. Xiang, Z. Liu, M. Wu, H. Liu, X. Zhang, Z. Wang, Z.L. Wang, L. Li, Enhanced Piezo-Photoelectric Catalysis with Oriented Carrier Migration in Asymmetric Au–ZnO Nanorod Array, *Small*, 16 (2020) 1907603.
- [35] Z. Wang, R. Yu, C. Pan, Z. Li, J. Yang, F. Yi, Z.L. Wang, Light-induced pyroelectric effect as an effective approach for ultrafast ultraviolet nanosensing, *Nature Communications*, 6 (2015) 8401.
- [36] Z. Liu, L. Wang, X. Yu, J. Zhang, R. Yang, X. Zhang, Y. Ji, M. Wu, L. Deng, L. Li, Z.L. Wang, Piezoelectric-Effect-Enhanced Full-Spectrum Photoelectrocatalysis in p–n Heterojunction, *Adv. Funct. Mater.*, 29 (2019) 1807279.
- [37] Z. Liang, C.-F. Yan, S. Rtimi, J. Bandara, Piezoelectric materials for catalytic/photocatalytic removal of pollutants: Recent advances and outlook, *Applied Catalysis B: Environmental*, 241 (2019) 256-269.

- [38] H. Li, Y. Sang, S. Chang, X. Huang, Y. Zhang, R. Yang, H. Jiang, H. Liu, Z.L. Wang, Enhanced Ferroelectric-Nanocrystal-Based Hybrid Photocatalysis by Ultrasonic-Wave-Generated Piezophototronic Effect, *Nano Lett.*, 15 (2015) 2372-2379.
- [39] Q. Liu, Z. Wang, H. Chen, H.-Y. Wang, H. Song, J. Ye, Y. Weng, Rules for Selecting Metal Cocatalyst Based on Charge Transfer and Separation Efficiency between ZnO Nanoparticles and Noble Metal Cocatalyst Ag/ Au/ Pt, *ChemCatChem*, 12 (2020) 3838-3842.
- [40] L. Wang, S. Liu, Z. Wang, Y. Zhou, Y. Qin, Z.L. Wang, Piezotronic Effect Enhanced Photocatalysis in Strained Anisotropic ZnO/TiO₂ Nanoplatelets via Thermal Stress, *ACS Nano*, 10 (2016) 2636-2643.
- [41] L. Zhu, Z.L. Wang, Recent Progress in Piezo-Phototronic Effect Enhanced Solar Cells, *Adv. Funct. Mater.*, 29 (2019) 1808214.

Highlights

- Plasmonic bimetallic ZnO nanorod array is fabricated for improving piezo-photocatalysis.
- The directional piezo-potential promotes the separation of carriers.
- The alignment of the Fermi level guides the directional migration of carriers.
- The coupling among LSPR effect, piezoelectricity and photocatalysis realizes optimal catalytic performance.

Declaration of interests

The authors declare that they have no known competing financial interests or personal relationships that could have appeared to influence the work reported in this paper.

The authors declare the following financial interests/personal relationships which may be considered as potential competing interests:

Journal Pre-proof